Research Article

Weidong Lei, Muhammad Ahsan, Waqas Khan, Zaheer Uddin*, and Masood Ahmad

A numerical Haar wavelet-finite difference hybrid method and its convergence for nonlinear hyperbolic partial differential equation

https://doi.org/10.1515/dema-2022-0203
received July 8, 2021; accepted January 20, 2023

Abstract: In this research work, we proposed a Haar wavelet collocation method (HWCM) for the numerical solution of first- and second-order nonlinear hyperbolic equations. The time derivative in the governing equations is approximated by a finite difference. The nonlinear hyperbolic equation is converted into its full algebraic form once the space derivatives are replaced by the finite Haar series. Convergence analysis is performed both in space and time, where the computational results follow the theoretical statements of convergence. Many test problems with different nonlinear terms are presented to verify the accuracy, capability, and convergence of the proposed method for the first- and second-order nonlinear hyperbolic equations.

Keywords: Haar wavelet, hyperbolic equation, collocation method, single- and double-soliton wave

MSC 2020: 35Exx, 65Mxx, 65Nxx, 00A69, 65T60, 35-XX, 65H05, 35C08

1 Introduction

Most of the scientific and physical phenomena govern the nonlinear hyperbolic partial differential equations (NLHPDEs) and have an important place in atomic physics, aerospace, industry, biology, and engineering problems. To find the exact solution of these kinds of NLHPDEs is very complicated due to the nonlinear term; therefore, implementation of numerical schemes is an alternative option to find their solution. In this article, we consider the first- and second-order NLHPDEs.

The first-order NLHPDEs can also be used in modeling the vibration of structures (like machines, buildings, and beams) and are considered as the foundation for the basic equations of atomic physics (see [1,2] and the references therein). Particular types of NLHPDEs are the Wave and Telegraph equations, which have wide applications in signal analysis for transmission, communication, and broadcasting of electric signals [3], random walk theory [4], and wave circulation or propagation [5].

* **Corresponding author: Zaheer Uddin,** Department of Basic Sciences, CECOS University of Information Technology and Emerging Sciences Peshawar, Peshawar 25000, Pakistan, e-mail: zaheeruddin@cecos.edu.pk
Weidong Lei: School of Civil and Environmental Engineering, Harbin Institute of Technology, Shenzhen, China
Muhammad Ahsan: School of Civil and Environmental Engineering, Harbin Institute of Technology, Shenzhen, China; Department of Mathematics, University of Swabi, Swabi 23430, Pakistan, e-mail: ahsankog@uoswabi.edu.pk
Waqas Khan: Department of Mathematics, University of Swabi, Swabi 23430, Pakistan
Masood Ahmad: Department of Basic Sciences, University of Engineering and Technology, Peshawar, Pakistan

The second-order NLHPDEs have many applications in mathematical chemistry, mathematical physics, and mathematical biology, such as chemical kinetics, fluid dynamics, solid state physics, quantum field theory, optics, atomic physics, and plasma physics.

Due to the aforementioned applications, different numerical techniques have been developed to solve the important NLHPDEs. These numerical techniques are the finite difference method [6–10], the Galerkin method [1,11–13], the B-spline collocation method [14], the spectral collocation method [15,16], the Chebyshev approach [17], and the wavelet collocation method [2]. Some recent contributions are also reported in [18–20].

Recently, the research has been focused on the Haar wavelet application in the investigation and analysis of different problems in applied sciences. Different algorithms based on weak and strong formulations contain the meshless wavelet method [21], the Daubechies wavelet-based method [22], the wavelet Galerkin method [23], and the wavelet collocation method [24,25]. A thorough introduction of the wavelet schemes for PDEs is given in [26]. Different scientific and engineering phenomena have been represented in the forms of ordinary differential equations, integro-differential equations, and PDEs, which have been solved by Haar wavelets in the references [27–42]. A further development of Haar wavelet is related to the solution of challenging fractional differential and integral equations [43–47]. The further extensions of the Haar wavelet approach are presented to solve linear and nonlinear direct problems [25,48–50] and inverse problems [41,42,51–53]. The latest contribution on Haar wavelets is presented in [54] for identification of software piracy.

Haar wavelets-based algorithms have also been reported for hyperbolic PDEs. In [55], a second-order linear hyperbolic PDE has been solved with the Haar wavelet operational matrix method. In [56], $\frac{\partial^3\varphi(s,\tau)}{\partial\tau\partial s^2}$ has been approximated by Haar wavelets to just find the numerical solution in the unit interval $[0, 1]$ using some transformation that converted the governing equation into the system of PDEs.

1.1 The governing equations

Mathematically, the first-order NLHPDE can be presented as follows:

$$\frac{\partial\varphi(s,\tau)}{\partial\tau} + \frac{\partial\varphi(s,\tau)}{\partial s} + f(\varphi(s,\tau)) = g(s,\tau), \quad a \le s \le b, \quad 0 \le \tau \le T, \tag{1}$$

with the initial and boundary conditions $\varphi(s, 0) = I(s)$ and $\varphi(a, \tau) = B(\tau)$.

The second-order NLHPDE can be written as follows:

$$\frac{\partial^2\varphi(s,\tau)}{\partial\tau^2} + \frac{\partial^2\varphi(s,\tau)}{\partial s^2} + f\left(\varphi(s,\tau), \frac{\partial\varphi(s,\tau)}{\partial\tau}\right) = g(s,\tau), \quad a \le s \le b, \quad 0 \le \tau \le T, \tag{2}$$

with the initial conditions

$$\varphi(s, 0) = I_1(s), \quad \frac{\partial\varphi(s,0)}{\partial\tau} = I_2(s)$$

and boundary conditions

$$\varphi(a, \tau) = B_1(\tau), \quad \varphi(b, \tau) = B_2(\tau).$$

In the above equations, f represents the nonlinear term, g, I, I_1, I_2, B, B_1, and B_2 are known functions, and φ is the only unknown function that is to be determined.

When $f\left(\varphi(s,\tau), \frac{\partial\varphi(s,\tau)}{\partial\tau}\right) = \frac{\partial\varphi(s,\tau)}{\partial\tau}$, equation (2) is known as the damped wave equation, whereas when $f\left(\varphi(s,\tau), \frac{\partial\varphi(s,\tau)}{\partial\tau}\right) = \frac{\partial\varphi(s,\tau)}{\partial\tau} + \varphi(s,\tau)$, equation (2) is known as the telegraph equation. These damped wave and telegraph equations have applications like wave phenomena and electric signal propagation in transmission wires. In fact, this partial differential equation is more appropriate than the ordinary diffusion

equation for representing the reaction-diffusion models in many scientific fields, such as biology, where biologists come across these types of equations in the development of pulsating blood flow in arteries and the random motion of bugs along a hedge [57].

If $f\left(\varphi(s,\tau), \frac{\partial\varphi(s,\tau)}{\partial\tau}\right) = \varphi(s,\tau) + \varphi(s,\tau)^k$, where $k = 2$ or 3, then equation (2) is named Klein-Gordon equation and can be studied in field theory and relativistic quantum mechanics, which have enormous significance for physicists [58] and also described dissemination of dislocations in crystals and the activities of basic particles.

When $f\left(\varphi(s,\tau), \frac{\partial\varphi(s,\tau)}{\partial\tau}\right) = \sin(\varphi(s,\tau))$, equation (2) is classified as Sine-Gordon equation, which has importance in a range of relevant fields, such as relativistic field theory and differential geometry, and it also appears in other related physics topics, including the movement of a rigid pendulum attached to an expanded cable, the transmission of fluxons in Josephson junctions, the transmission in ferromagnetic materials of waves taking rotary motions in the course of magnetization, laser pulses in two-state medium and dislocations in crystals [59,60].

In this article, the potential of Haar wavelets is investigated on the first- and second-order NLHPDEs. The theoretical convergence is supported by our numerical results in the interval [a, b]. The time and space derivatives are discretized using finite-difference and Haar wavelets, respectively. Due to the discontinuity of the Haar functions, the approximation starts from the highest-order derivatives in the model equation. By further integration of the series, the unknown solution can be obtained. By introducing these approximations in equation (1) or (2), a system of algebraic equations can be easily solved. The details of the proposed methods are given in the subsequent sections.

2 Haar functions

A generalized representation of the Haar functions is defined as follows:

$$h_i(s) = \begin{cases} 1 & \text{for} \quad s \in [\zeta_1(i), \zeta_2(i)), \\ -1 & \text{for} \quad s \in [\zeta_2(i), \zeta_3(i)), \\ 0 & \text{elsewhere,} \end{cases}$$

where

$$\zeta_1(i) = a + \frac{(b-a)k}{m}, \quad \zeta_2(i) = a + \frac{(b-a)(k+0.5)}{m}, \quad \zeta_3(i) = a + \frac{(b-a)(k+1)}{m}.$$

Here, $m = 2^j$, $j = 0, 1, \ldots$, represents the level of the wavelet, $k = 0, 1, \ldots, m-1$ is the translation parameter, and $i = m + k + 1$. We note that $i \geq 2$. We define

$$h_1(s) = \begin{cases} 1 & \text{for} \quad s \in [a, b], \\ 0 & \text{elsewhere,} \end{cases}$$

which is also known as the mother wavelet. To keep the derivations simple, we intend to introduce some notations for the following integrals for $i = 2, 3, 4, \ldots$,

$$p_{i,1}(s) = \int_a^s h_i(s')\mathrm{d}s'$$
$$= \begin{cases} 0 & \text{for} \quad s < \zeta_1(i), \\ s - \zeta_1(i) & \text{for} \quad s \in [\zeta_1(i), \zeta_2(i)), \\ s - \zeta_1(i) - 2(s - \zeta_2(i)) & \text{for} \quad s \in [\zeta_2(i), \zeta_3(i)), \\ s - \zeta_1(i) - 2(s - \zeta_2(i)) + (s - \zeta_3(i)) & \text{for} \quad s \geq \zeta_3(i), \end{cases}$$
$$p_{i,2}(s) = \int_a^s p_{i,1}(s')\mathrm{d}s'$$
$$= \begin{cases} 0 & \text{for} \quad s < \zeta_1(i), \\ \frac{1}{2}(s - \zeta_1(i))^2 & \text{for} \quad s \in [\zeta_1(i), \zeta_2(i)), \\ \frac{1}{2}[(s - \zeta_1(i))^2 - 2(s - \zeta_2(i))^2] & \text{for} \quad s \in [\zeta_2(i), \zeta_3(i)), \\ \frac{1}{2}[(s - \zeta_1(i))^2 - 2(s - \zeta_2(i))^2 + (s - \zeta_3(i))^2] & \text{for} \quad s \geq \zeta_3(i), \end{cases}$$

and

$$C = \int_a^b p_{i,1}(s')\mathrm{d}s' = \frac{(b-a)^2}{4m^2}. \tag{3}$$

As $p_{i,1}(s)$ is increasing in the interval $[\zeta_1(i), \zeta_2(i))$ and decreasing in the interval $[\zeta_2(i), \zeta_3(i))$, but the maximum value is at $\zeta_2(i)$. Hence,

$$\max_s(p_{i,1}(s)) = p_{i,1}(\zeta_2(i)) = \frac{b-a}{2m}. \tag{4}$$

It is noteworthy to mention that the following formula has been proved in [61]:

$$\max_s(p_{i,2}(s)) = \frac{(b-a)^2}{4m^2}. \tag{5}$$

3 Haar approximation

As we consider here the first- and second-order NLHPDEs, we approximate them with two different Haar wavelet collocation methods (HWCMs) in Sections 3.1 and 3.2.

3.1 HWCM for first-order NLHPDE

In this subsection, we consider Haar wavelets as a basic part of our numerical technique for the spatial discretization of equation (1). To construct HWCM for first-order NLHPDE, we start approximating the first-order derivative with Haar functions as follows:

$$\frac{\partial\varphi(s,\tau)}{\partial s} = \sum_{i=1}^{\infty}\lambda_i(\tau)h_i(s). \tag{6}$$

Integrating equation (6) w.r.t s, from a to s, we obtain

$$\varphi(s,\tau) = \varphi(a,\tau) + \sum_{i=1}^{\infty}\lambda_i(\tau)p_{i,1}(s).$$

If τ_n be the current time level and τ_{n+1} be the next time level, then equation (1) can be linearized in the following manner:

$$\frac{\partial\varphi(s,\tau_{n+1})}{\partial\tau} + \frac{\partial\varphi(s,\tau_{n+1})}{\partial s} + f(\varphi(s,\tau_n)) = g(s,\tau_{n+1}).$$

Using the forward difference approximation for time derivative, we obtain

$$\frac{\varphi(s,\tau_{n+1}) - \varphi(s,\tau_n)}{\Delta\tau} + \frac{\partial\varphi(s,\tau_{n+1})}{\partial s} + f(\varphi(s,\tau_n)) = g(s,\tau_{n+1}) - O(\Delta\tau). \tag{7}$$

For a Haar wavelet-based numerical solution, we define $M = 2^J$ for some $J > 0$ and

$$\varphi_M(s,\tau) = \varphi(a,\tau) + \sum_{i=1}^{2M}\lambda_i(\tau)p_{i,1}(s). \tag{8}$$

If $j = J$, then $k = 2^J - 1$ and $i = m + k + 1 = 2^J + 2^J - 1 + 1 = 2 \times 2^J = 2M$ (Section 2). Differentiating equation (8) w.r.t s, we obtain

$$\frac{\partial\varphi_M(s,\tau)}{\partial s} = \sum_{i=1}^{2M}\lambda_i(\tau)h_i(s).$$

The relationship between exact and approximate representations is

$$\varphi(s,\tau) = \varphi_M(s,\tau) + E_M(s,\tau), \quad \text{and} \quad \frac{\partial\varphi(s,\tau)}{\partial s} = \frac{\partial\varphi_M(s,\tau)}{\partial s} + \frac{\partial E_M(s,\tau)}{\partial s},$$

$$\text{where} \quad E_M(s,\tau) = \sum_{i=2M+1}^{\infty}\lambda_i(\tau)p_{i,1}(s) \quad \text{and} \quad \frac{\partial E_M(s,\tau)}{\partial s} = \sum_{i=2M+1}^{\infty}\lambda_i(\tau)h_i(s).$$

Now the exact form of equation (7) using Haar wavelet is

$$\begin{aligned}
&\frac{\varphi_M(s,\tau_{n+1}) - \varphi_M(s,\tau_n)}{\Delta\tau} + \frac{E_M(s,\tau_{n+1}) - E_M(s,\tau_n)}{\Delta\tau} + \frac{\partial\varphi_M(s,\tau_{n+1})}{\partial s} + \frac{\partial E_M(s,\tau_{n+1})}{\partial s} + f(\varphi_M(s,\tau_n)) + f(E_M(s,\tau_n))\\
&\quad = g(s,\tau_{n+1}) - O(\Delta\tau),\\
&\frac{\varphi_M(s,\tau_{n+1}) - \varphi_M(s,\tau_n)}{\Delta\tau} + \frac{\partial\varphi_M(s,\tau_{n+1})}{\partial s} + f(\varphi_M(s,\tau_n)) = g(s,\tau_{n+1}) - O(\Delta\tau) - \frac{E_M(s,\tau_{n+1}) - E_M(s,\tau_n)}{\Delta\tau}\\
&\qquad\qquad - \frac{\partial E_M(s,\tau_{n+1})}{\partial s} - f(E_M(s,\tau_n)).
\end{aligned}$$

Dropping all the error terms and using the collocation points $s_l = a + (b-a)\frac{(l-0.5)}{2M}$, $l = 1, 2, \ldots, 2M$, we have

$$\frac{\varphi_M(s_l,\tau_{n+1}) - \varphi_M(s_l,\tau_n)}{\Delta\tau} + \frac{\partial\varphi_M(s_l,\tau_{n+1})}{\partial s} + f(\varphi_M(s_l,\tau_n)) = g(s_l,\tau_{n+1}).$$

Now defining

$$\mathcal{P}^n_{M,l} \coloneqq \varphi(a,\tau) + \sum_{i=1}^{2M}\lambda_i^{M,n}p_{i,1}(s_l), \quad \text{and} \quad \frac{\partial\mathcal{P}^n_{M,l}}{\partial s} \coloneqq \sum_{i=1}^{2M}\lambda_i^{M,n}h_i(s_l), \tag{9}$$

we obtain

$$\frac{\mathcal{P}^{n+1}_{M,l} - \mathcal{P}^n_{M,l}}{\Delta\tau} + \frac{\partial\mathcal{P}^{n+1}_{M,l}}{\partial s} + f(\mathcal{P}^n_{M,l}) = g(s_l,\tau_{n+1}). \tag{10}$$

Putting equation (9) in equation (10), we obtain a system of $2M$ equations with $2M$ unknowns, which can be easily solved for λ_is, i.e.,

$$\lambda_i^{M,n+1}(p_{i,1}(s_l) + \Delta\tau h_i(s_l)) = \mathcal{P}_{M,l}^n + \Delta\tau g(s_l, \tau_{n+1}) - \Delta\tau f(\mathcal{P}_{M,l}^n) - \varphi(a, \tau). \tag{11}$$

Equation (11) can be written as follows:

$$[\mathcal{H}]_{2M\times 2M}[\mathcal{X}]_{2M\times 1} = [B]_{2M\times 1}, \tag{12}$$

where $\mathcal{H}$ is the Haar coefficient matrix,$\mathcal{X} = [\lambda_1^{M,n+1}\lambda_2^{M,n+1} \dots \lambda_{2M}^{M,n+1}]$ is the unknown Haar wavelet coefficients, and B is a vector that represents the right side of equation (11). Equation (12) can be easily solved for $\mathcal{X}$. By inserting $\mathcal{X}$ in equation (9), we obtain the desired numerical solution. We define the following formula to interpolate the solution at any point s:

$$\mathcal{P}_M^{n+1}(s) \coloneqq \varphi(a, \tau_{n+1}) + \sum_{i=1}^{2M}\lambda_i^{M,n+1}p_{i,1}(s),$$

then $\mathcal{P}_M^{n+1}(s) \approx \varphi(s, \tau_{n+1})$.

3.2 HWCM for second-order NLHPDE

To construct HWCM for second-order NLHPDE, we start by approximating the second-order derivative with Haar functions as follows:

$$\frac{\partial^2\varphi(s, \tau)}{\partial s^2} = \sum_{i=1}^{\infty}\lambda_i(\tau)h_i(s). \tag{13}$$

Integrating equation (13) w.r.t s, from a to s, we obtain

$$\frac{\partial\varphi(s, \tau)}{\partial s} = \frac{\partial\varphi(a, \tau)}{\partial s} + \sum_{i=1}^{\infty}\lambda_i(\tau)p_{i,1}(s). \tag{14}$$

Integrating equation (14) w.r.t s, from a to b, we obtain

$$\frac{\partial\varphi(a, \tau)}{\partial s} = \frac{\varphi(b, \tau) - \varphi(a, \tau)}{b - a} - \sum_{i=1}^{\infty}\lambda_i(\tau)\frac{C}{b - a}. \tag{15}$$

Eliminating $\frac{\partial\varphi(a,\tau)}{\partial s}$ from equations (14) and (15), we obtain

$$\frac{\partial\varphi(s, \tau)}{\partial s} = \overline{w}_o(\tau) + \sum_{i=1}^{\infty}\lambda_i(\tau)\overline{h}_i(s), \tag{16}$$

where $\overline{w}_o(\tau) = \frac{\varphi(b,\tau)-\varphi(a,\tau)}{b-a}$ and $\overline{h}_i(s) = p_{i,1}(s) - \frac{C}{b-a}$. Again, partially integrating equation (16) w.r.t s, from a to s, we obtain

$$\begin{aligned}&\varphi(s, \tau) = \widetilde{w}_o(s, \tau) + \sum_{i=1}^{\infty}\lambda_i(\tau)\widetilde{h}_i(s),\\ &\text{where}\quad \widetilde{w}_o(s, \tau) = \varphi(a, \tau) + (s - a)\overline{w}_o(\tau), \quad \text{and}\quad \widetilde{h}_i(s) = p_{i,2}(s) - (s - a)\frac{C}{b - a}.\end{aligned} \tag{17}$$

If τ_n be the current time level and τ_{n+1} be the next time level, then equation (2) can be linearized in the following manner:

$$\frac{\partial^2\varphi(s, \tau_{n+1})}{\partial\tau^2} + \frac{\partial^2\varphi(s, \tau_{n+1})}{\partial s^2} + f_1(\varphi(s, \tau_n))\frac{\partial\varphi(s, \tau_{n+1})}{\partial\tau} = g(s, \tau_{n+1}),$$

where f_1 is the linearized form of the function f. Using forward difference approximation for time derivative, we obtain

$$\begin{aligned}&\frac{\varphi(s, \tau_{n+1}) - 2\varphi(s, \tau_n) + \varphi(s, \tau_{n-1})}{\Delta\tau^2} + \frac{\partial^2\varphi(s, \tau_{n+1})}{\partial s^2} + f_1(\varphi(s, \tau_n))\left(\frac{\varphi(s, \tau_{n+1}) - \varphi(s, \tau_n)}{\Delta\tau}\right)\\ &= g(s, \tau_{n+1}) - O(\Delta\tau^2) - O(\Delta\tau).\end{aligned} \tag{18}$$

To find the numerical solution based on Haar wavelet, we define

$$\varphi_M(s,\tau) = \widetilde{w}_o(s,\tau) + \sum_{i=1}^{2M}\lambda_i(\tau)\widetilde{h}_i(s). \tag{19}$$

Differentiating equation (19) w.r.t s, we obtain

$$\frac{\partial\varphi_M(s,\tau)}{\partial s} = \overline{w}_o(\tau) + \sum_{i=1}^{2M}\lambda_i(\tau)\overline{h}_i(s), \quad \frac{\partial^2\varphi_M(s,\tau)}{\partial s^2} = \sum_{i=1}^{2M}\lambda_i(\tau)h_i(s).$$

The relationship between exact and approximate representations are

$$\varphi(s,\tau) = \varphi_M(s,\tau) + E_M(s,\tau), \quad \text{where } E_M(s,\tau) = \sum_{i=2M+1}^{\infty}\lambda_i(\tau)\widetilde{h}_i(s),$$
$$\frac{\partial\varphi(s,\tau)}{\partial s} = \frac{\partial\varphi_M(s,\tau)}{\partial s} + \frac{\partial E_M(s,\tau)}{\partial s}, \quad \text{where } \frac{\partial E_M(s,\tau)}{\partial s} = \sum_{i=2M+1}^{\infty}\lambda_i(\tau)\overline{h}_i(s),$$

and

$$\frac{\partial^2\varphi(s,\tau)}{\partial s^2} = \frac{\partial^2\varphi_M(s,\tau)}{\partial s^2} + \frac{\partial^2 E_M(s,\tau)}{\partial s^2}, \quad \text{where } \frac{\partial^2 E_M(s,\tau)}{\partial s^2} = \sum_{i=2M+1}^{\infty}\lambda_i(\tau)h_i(s).$$

Now, the exact form of equation (18) using Haar wavelet is

$$\begin{aligned}&\frac{\varphi_M(s,\tau_{n+1}) - 2\varphi_M(s,\tau_n) + \varphi_M(s,\tau_{n-1})}{\Delta\tau^2} + \frac{\partial^2\varphi_M(s,\tau_{n+1})}{\partial s^2} + f_1(\varphi_M(s,\tau_n))\left(\frac{\varphi_M(s,\tau_{n+1}) - \varphi_M(s,\tau_n)}{\Delta\tau}\right)\\ &= g(s,\tau_{n+1}) - \frac{E_M(s,\tau_{n+1}) - 2E_M(s,\tau_n) + E_M(s,\tau_{n-1})}{\Delta\tau^2} - \frac{\partial^2 E_M(s,\tau_{n+1})}{\partial s^2} - f_1(E_M(s,\tau_n))\left(\frac{E_M(s,\tau_{n+1}) - E_M(s,\tau_n)}{\Delta\tau}\right)\\ &\quad - O(\Delta\tau).\end{aligned}$$

Dropping all the error terms and using the collocation points $s_l = a + (b-a)\frac{(l-0.5)}{2M}$, $l = 1, 2, \ldots, 2M$, we have

$$\frac{\varphi_M(s_l,\tau_{n+1}) - 2\varphi_M(s_l,\tau_n) + \varphi_M(s_l,\tau_{n-1})}{\Delta\tau^2} + \frac{\partial^2\varphi_M(s_l,\tau_{n+1})}{\partial s^2} + f_1(\varphi_M(s_l,\tau_n))\left(\frac{\varphi_M(s_l,\tau_{n+1}) - \varphi_M(s_l,\tau_n)}{\Delta\tau}\right) = g(s_l,\tau_{n+1}).$$

Now defining

$$\begin{aligned}\mathcal{P}^n_{M,l} &\coloneqq \widetilde{w}_o(s_l,\tau_n) + \sum_{i=1}^{2M}\lambda_i^{M,n}\widetilde{h}_i(s_l),\\ \frac{\partial\mathcal{P}^n_{M,l}}{\partial s} &\coloneqq \overline{w}_o(\tau_n) + \sum_{i=1}^{2M}\lambda_i^{M,n}\overline{h}_i(s_l),\\ \frac{\partial^2\mathcal{P}^n_{M,l}}{\partial s^2} &\coloneqq \sum_{i=1}^{2M}\lambda_i^{M,n}h_i(s_l),\end{aligned} \tag{20}$$

we obtain

$$\frac{\mathcal{P}^{n+1}_{M,l} - 2\mathcal{P}^n_{M,l} + \mathcal{P}^{n-1}_{M,l}}{\Delta\tau^2} + \frac{\partial^2\mathcal{P}^{n+1}_{M,l}}{\partial s^2} + f_1(\mathcal{P}^n_{M,l})\left(\frac{\mathcal{P}^{n+1}_{M,l} - \mathcal{P}^n_{M,l}}{\Delta\tau}\right) = g(s_l,\tau_{n+1}). \tag{21}$$

Putting equation (20) in equation (21), we obtain a system of $2M$ equations with $2M$ unknowns as follows:

$$[\mathcal{H}]_{2M\times 2M}[\mathcal{X}]_{2M\times 1} = [B]_{2M\times 1}, \tag{22}$$

where $\mathcal{H}$ is the Haar coefficient matrix,$\mathcal{X} = [\lambda_1^{M,n+1}\lambda_2^{M,n+1}\ldots\lambda_{2M}^{M,n+1}]$ is the unknown Haar wavelet coefficients and B is a vector that represents the right side of equation (21). The equation (22) can be easily solved

for $\mathcal{X}$. By using $\mathcal{X}$ in equation (20), one can obtain the desired numerical solution. We define the following formula to interpolate the solution at any point s,

$$\mathcal{P}_M^{n+1}(s) \coloneqq \widetilde{w}_0(s, \tau_{n+1}) + \sum_{i=1}^{2M} \lambda_i^{M,n+1} \widetilde{h}_i(s),$$

then $\mathcal{P}_M^{n+1}(s) \approx \varphi(s, \tau_{n+1})$.

3.3 Summary of the algorithms

The algorithm for the first- and second-order NLHPDEs is presented as follows:

Input: $N = 2M$, $M = 2^J$, $J \in \mathbb{N}_0$.

Step 1: Compute $h_i(x)$, $p_{i,1}(x)$ and $p_{i,2}(x)$.

For $n = 1, \ldots, P$, where P is the maximum number of iteration.

Step 2: Construct $\mathcal{H}$ and B according to equations (12) or (22).

Step 3: Calculate the unknown Haar wavelet coefficients with the help of

$$\mathcal{X} = \mathcal{H}^{-1}B.$$

Step 4: Construct an approximate solution from equations (9) or (20).

Output: If the maximum of absolute error is acceptable, then the for loop will end; otherwise, go to Step 2.

4 Convergence analysis

Let $[0, T]$ be partitioned into $0 = \tau_0 < \tau_1 < \ldots \tau_P = T$, where P is a positive integer. In this section, we derive the rate of convergence when $\varphi(s, \tau_P)$ is approximated by the solution given by the numerical method designed in Section 3.

Theorem 1. *Assume that* $\frac{\partial \varphi}{\partial \tau}$, $\frac{\partial \varphi}{\partial s}$, *and* $\frac{\partial^2 \varphi}{\partial s^2}$ *exist and are bounded in* $[a, b] \times [0, T]$. *For any* $M = 2^J$, $J = 0, 1, 2, \ldots$, *and* $p = 0, 1, \ldots P$, *where* P *is a positive integer, if* $\mathcal{P}_M^p(s)$ *is the Haar wavelet solution and* $\varphi(s, \tau_p)$ *is the exact solution, then*

$$\max_{0 \le p \le P} \|\varphi(.,\tau_p) - \mathcal{P}_M^p\|_{L^\infty(a,b)} \le O\left(\frac{1}{M}\right) + O(\Delta\tau), \quad \text{as } J \to \infty \quad \text{and} \quad P \to \infty,$$

where $\Delta\tau = \max_{0 \le p \le P-1}(\tau_{p+1} - \tau_p)$.

Proof. For $p = 1, 2, \ldots, P$, we have

$$\|\varphi(.,\tau_p) - \mathcal{P}_M^p\|_{L^\infty(a,b)} \le \|E_M\|_{L^\infty(a,b)} + \|\varphi_M(.,\tau_p) - \mathcal{P}_M^p\|_{L^\infty(a,b)},$$

where $\|E_M\|_{L^\infty(a,b)}$ is defined as follows:

$$\|E_M\|_{L^\infty(a,b)} \coloneqq \|\varphi(.,\tau_p) - \varphi_M(.,\tau_p)\|_{L^\infty(a,b)} = \max_s \left| \sum_{i=2M+1}^{\infty} \lambda_i p_{i,1}(s) \right|.$$

It is shown in [61, equation (18)] that $\lambda_i \le \beta/2^{j+1}$. In fact, it can be shown that $|\lambda_i| \le \beta/2^{j+1}$ (which should also have been required in [61]). Therefore,

$$\|E_M\|_{L^\infty(a,b)} \le \beta \sum_{i=2M+1}^{\infty} \frac{1}{2^{j+1}} \max_s |p_{i,1}(s)|.$$

By using equation (4), we obtain

$$\begin{aligned}\|E_M\|_{L^\infty(a,b)} &\le \beta \sum_{i=2M+1}^{\infty} \frac{1}{2^{j+1}} \max_s |p_{i,1}(s)| \\ &\le \beta(b-a) \sum_{i=2M+1}^{\infty} \left(\frac{1}{2^{j+1}}\right)^2 \\ &\le \beta(b-a) \sum_{j=J+1}^{\infty} \sum_{k=0}^{2^j-1} \left(\frac{1}{2^{j+1}}\right)^2 \\ &= \frac{\beta(b-a)}{2} \sum_{j=J+1}^{\infty} \frac{1}{2^{j+1}} \\ &\le \frac{\beta(b-a)}{4} \frac{1}{2^{J+1}} = \frac{\beta(b-a)}{4M},\end{aligned}$$

where $b-a$ is the length of the interval, $M = 2^J$, and $b-a \ll M$ when $J \to \infty$, so

$$\|E_M\|_{L^\infty(a,b)} \le O\left(\frac{1}{M}\right).$$

The second part $\|\varphi_M(.,\tau_p) - \mathcal{P}_M^p\|_{L^\infty(a,b)}$ is the error due to the time iteration where we used forward difference approximation, which is the first-order accurate in time, i.e., $\|\varphi_M(.,\tau_p) - \mathcal{P}_M^p\| \le O(\Delta\tau)$. □

Theorem 2. *Assume that* $\frac{\partial\varphi}{\partial\tau}$, $\frac{\partial^2\varphi}{\partial\tau^2}$, $\frac{\partial w}{\partial s}$, $\frac{\partial^2 w}{\partial s^2}$, *and* $\frac{\partial^3 w}{\partial s^3}$ *exist and are bounded in* $[a,b]\times[0,T]$. *For any* $M = 2^J$, $J = 0, 1, 2, \dots$, *and* $p = 0, 1, \dots P$, *where* P *is a positive integer, if* $\mathcal{P}_M^p(s)$ *is the Haar wavelet solution and* $\varphi(s,\tau_p)$ *is the exact solution, then*

$$\max_{0\le p\le P} \|\varphi(.,\tau_p) - \mathcal{P}_M^p\|_{L^\infty(a,b)} \le O\left(\frac{1}{M^2}\right) + O(\Delta\tau), \ \text{as } J\to\infty \text{ and } P\to\infty,$$

where $\Delta\tau = \max_{0\le p\le P-1}(\tau_{p+1} - \tau_p)$.

Proof. For $p = 1, 2, \dots, P$, we have

$$\|\varphi(.,\tau_p) - \mathcal{P}_M^p\|_{L^\infty(a,b)} \le \|E_M\|_{L^\infty(a,b)} + \|\varphi_M(.,\tau_p) - \mathcal{P}_M^p\|_{L^\infty(a,b)},$$

where $\|E_M\|_{L^\infty(a,b)}$ is defined as follows:

$$\|E_M\|_{L^\infty(a,b)} := \|\varphi(.,\tau_p) - \varphi_M(.,\tau_p)\|_{L^\infty(a,b)} = \max_s \left| \sum_{i=2M+1}^{\infty} \lambda_i \tilde{h}_i(s) \right|.$$

$$\|E_M\|_{L^\infty(a,b)} \le \beta \sum_{i=2M+1}^{\infty} \frac{1}{2^{j+1}} \max_s |\tilde{h}_i(s)|.$$

By using successively equation (17), the triangle inequality, equations (3) and (5), we obtain

$$\begin{aligned}\|E_M\|_{L^\infty(a,b)} &\le \beta \sum_{i=2M+1}^{\infty} \frac{1}{2^{j+1}} \left[\max_s \left| (p_{i,2}(s)) \right| + \max_s |(s-a)\frac{C}{b-a}| \right] \\ &\le 2\beta(b-a)^2 \sum_{i=2M+1}^{\infty} \left(\frac{1}{2^{j+1}}\right)^3 \\ &\le 2\beta(b-a)^2 \sum_{j=J+1}^{\infty} \sum_{k=0}^{2^j-1} \left(\frac{1}{2^{j+1}}\right)^3 \\ &= \beta(b-a)^2 \sum_{j=J+1}^{\infty} \left(\frac{1}{2^{j+1}}\right)^2 \\ &\le \frac{\beta(b-a)^2}{3} \left(\frac{1}{2^{J+1}}\right)^2 = O\left(\frac{1}{M^2}\right).\end{aligned}$$

The second part $\|\varphi_M(.,\tau_p) - \mathcal{P}_M^p\|_{L^\infty(a,b)}$ is the error due to the time iteration where we used a finite difference approximation that is first-order accurate in time, i.e., $\|\varphi_M(.,\tau_p) - \mathcal{P}_M^p\| \le O(\Delta\tau)$. □

5 Test cases

We implement the HWCM by calculating the results of different numerical test problems. The E_∞ error norm has been used for accuracy measurements, which is defined as follows:

$$E_\infty = \max_{1\le l\le 2M} (|\varphi(s_l, \tau_P) - \mathcal{P}_{M,l}^P|).$$

All results were obtained by "MATLAB R2009b" software on DELL PC Laptop (Intel(R) Core(TM)i3-3110M CPU 2.40 GHz, 4.0 GB RAM). For all computations, we used CPU time having the unit "second."

Test Problem 1. We consider the following linear case of first-order hyperbolic equation with $f(\varphi(s,\tau)) = \varphi(s,\tau)$ in equation (1):

$$\frac{\partial\varphi}{\partial\tau} + \frac{\partial\varphi}{\partial s} + \varphi = g(s,\tau), \quad a \le s \le b, \quad 0 \le \tau \le T,$$

with the initial and boundary conditions,

$$\varphi(s,0) = \cos(s) \quad \text{and} \quad \varphi(a,\tau) = \cos(a+\tau),$$

where

$$g(s,\tau) = -2\sin(s+\tau) + \cos(s+\tau).$$

The exact solution is given in [1,2]

$$\varphi(s,\tau) = \cos(s+\tau).$$

Tables 1 and 2 describe the maximum error, the convergence, and the CPU time. The theoretical rate of convergence is 1 (Theorem 1), which is in good agreement with the experimental rate of convergence given in Table 1. The comparison of Haar wavelet-based solution with the exact solution and the absolute error at different T are shown in Figure 1. From the aforementioned figures and tables, it is concluded that the proposed HWCM is efficient and accurate.

Table 1: The numerical results at $M = 16$, $a = 0$, $b = 1$, and $T = 1$ for Test Problem 1. The theoretical rate of convergence is 1 (Theorem 1)

$\Delta\tau$	E_∞	Experimental rate of convergence
1/10	0.0575	—
1/20	0.0290	0.9843
1/30	0.0195	0.9878
1/40	0.0146	0.9900
1/50	0.0117	0.9915
1/60	0.0098	0.9926
1/70	0.0084	0.9935
1/80	0.0074	0.9942
1/90	0.0065	0.9949
1/100	0.0059	0.9954

Table 2: The numerical results at $a = 0$, $b = 1$, and $T = 1$ for Test Problem 1 with different M

M	E_∞	CPU time
($\Delta\tau = 0.01$)		
1	1.579×10^{-2}	0.5020
2	6.605×10^{-3}	0.5312
4	5.791×10^{-3}	0.6467
8	5.851×10^{-3}	0.8029
16	5.890×10^{-3}	1.5616
($\Delta\tau = 0.001$)		
1	1.389×10^{-2}	0.5855
2	4.005×10^{-3}	0.7357
4	1.112×10^{-3}	1.1304
8	6.208×10^{-4}	3.0479
16	5.905×10^{-4}	7.2140

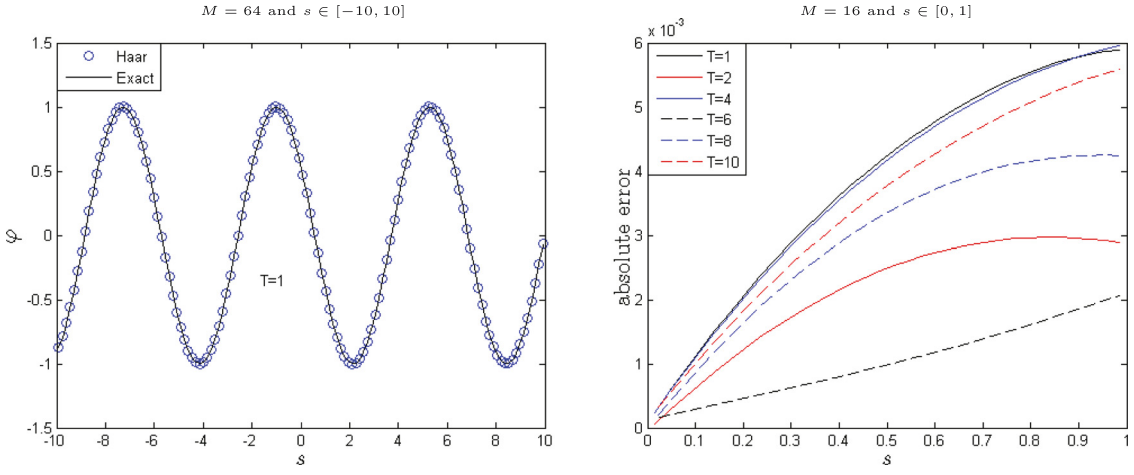

Figure 1: Numerical solutions for Test Problem 1 at different T with $\Delta\tau = 0.01$.

Test Problem 2. Now considering the following first-order NLHPDE with $f(\varphi(s,\tau)) = \sin(\varphi(s,\tau))$ in equation (1):

$$\frac{\partial\varphi}{\partial\tau} + \frac{\partial\varphi}{\partial s} + \sin(\varphi) = g(s,\tau), \quad a \le s \le b, \quad 0 \le \tau \le T,$$

with the initial and boundary conditions,

$$\varphi(s,0) = \sin(s) \quad \text{and} \quad \varphi(a,\tau) = \sin(a-\tau),$$

where

$$g(s,\tau) = \sin(\sin(s-\tau)).$$

The exact solution is

$$\varphi(s,\tau) = \sin(s-\tau).$$

Tables 3–6 illustrate the maximum error, the convergence, and the CPU time, where the accuracy of the solution depends on parameters M and $\Delta\tau$. The theoretical and experimental rates of convergence are inline, i.e., 1 (Theorem 1 and Table 6). The maximum errors for $T \le 10$ and $T > 10$ are given in Tables 3 and 4,

Table 3: The numerical results at $M = 16$, $a = 0$, $b = 1$, and $\Delta\tau = 0.01$ when $T \leq 10$ for Test Problem 2

T	1	2	4	6	8	10
E_∞	6.115×10^{-3}	2.112×10^{-3}	6.610×10^{-3}	4.947×10^{-3}	1.717×10^{-3}	6.808×10^{-3}
CPU time	1.060	1.988	3.982	5.954	7.913	9.852

Table 4: The numerical results at $M = 16$, $a = 0$, $b = 1$, and $\Delta\tau = 0.01$ when $T > 10$ for Test Problem 2

T	20	40	60	80	100
E_∞	5.624×10^{-3}	3.078×10^{-3}	6.477×10^{-3}	3.727×10^{-3}	4.122×10^{-3}
CPU time	12.550	26.065	38.383	50.015	62.849

Table 5: The numerical results at $a = 0$, $b = 1$, and $T = 1$ for Test Problem 2 with different M

M	E_∞	CPU time	E_∞	CPU time
($\Delta\tau = 0.01$)			($\Delta\tau = 0.001$)	
1	1.402×10^{-2}	0.050	1.485×10^{-2}	0.138
2	7.530×10^{-3}	0.093	5.070×10^{-3}	0.252
4	6.410×10^{-3}	0.111	1.455×10^{-3}	0.733
8	6.146×10^{-3}	0.315	7.933×10^{-4}	2.606
16	6.115×10^{-3}	1.060	6.649×10^{-4}	7.084

Table 6: The numerical results at $M = 16$, $a = 0$, $b = 1$, and $T = 1$ for Test Problem 2. The The theoretical rate of convergence is 1 (Theorem 1)

$\Delta\tau$	E_∞	Experimental rate of convergence
1/10	0.0562	—
1/20	0.0291	0.9492
1/30	0.0197	0.9621
1/40	0.0149	0.9682
1/50	0.0120	0.9717
1/60	0.0100	0.9739
1/70	0.0086	0.9754
1/80	0.0076	0.9764
1/90	0.0067	0.9771
1/100	0.0061	0.9775

and the algorithm gives stable results for $T \gg 10$. From these tables, it is concluded that as the resolution M increases and $\Delta\tau$ decreases, the accuracy of the proposed HWCM also increases.

Test Problem 3. We consider the following first-order NLHPDE with $f(\varphi(s,\tau)) = e^{\varphi(s,\tau)}$ in equation (1)

$$\frac{\partial\varphi}{\partial\tau} + \frac{\partial\varphi}{\partial s} + e^{\varphi} = g(s,\tau), \quad a \leq s \leq b, \quad 0 \leq \tau \leq T,$$

with the initial and boundary conditions,

$$\varphi(s,0) = s^2 - s \quad \text{and} \quad \varphi(a,\tau) = a^2 - a + \tau,$$

where

$$g(s, \tau) = 2s + e^{(s^2 - s + \tau)}.$$

The exact solution is

$$\varphi(s, \tau) = s^2 - s + \tau.$$

In Tables 7 and 8 the maximum error, the convergence, and the CPU time are displayed, where the precision of the solution depends on M and $\Delta\tau$. The theoretical and experimental rates of convergence are aligned, i.e., 1 (Theorem 1 and Table 8). Figure 2 depicts the space-time graph of approximate and exact

Table 7: The numerical results at $a = 0$, $b = 1$, and $T = 1$ for Test Problem 3 with different M

M	E_∞	CPU time	E_∞	CPU time
($\Delta\tau = 0.01$)			($\Delta\tau = 0.001$)	
1	4.499×10^{-2}	0.148	4.205×10^{-2}	0.231
2	1.439×10^{-3}	0.284	1.243×10^{-3}	0.435
4	8.217×10^{-3}	0.295	3.522×10^{-3}	0.934
8	7.714×10^{-3}	0.482	9.917×10^{-4}	2.719
16	7.625×10^{-3}	1.136	8.042×10^{-4}	10.030

Table 8: The numerical results at $M = 16$, $a = 0$, $b = 1$, and $T = 1$ for Test Problem 2. Theoretical rate of convergence is 1 (Theorem 1)

$\Delta\tau$	E_∞	Experimented rate of convergence
1/10	0.0765	—
1/20	0.0379	1.0103
1/30	0.0253	1.0021
1/40	0.0189	0.9991
1/50	0.0151	0.9974
1/60	0.0126	0.9962
1/70	0.0108	0.9953
1/80	0.0095	0.9946
1/90	0.0084	0.9939
1/100	0.0076	0.9933

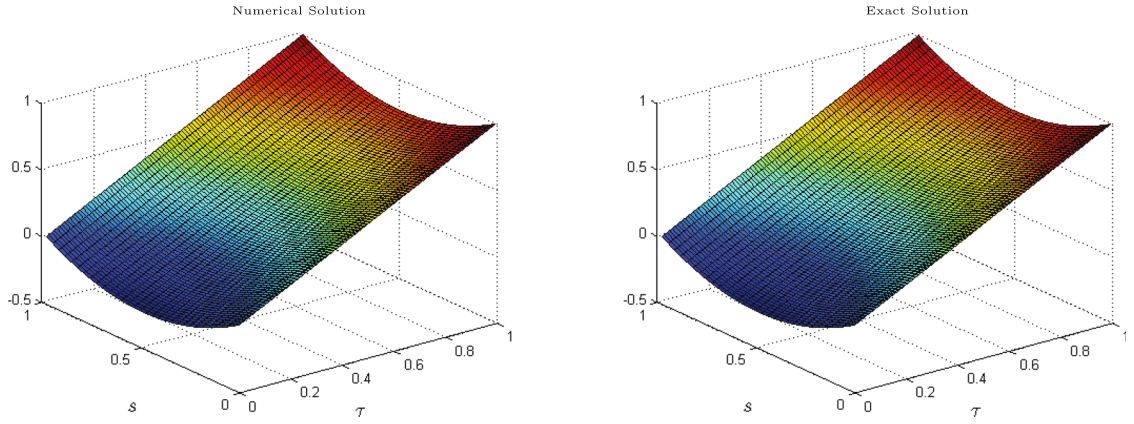

Figure 2: The 3D plots for Test Problem 3 at $M = 16$, $T = 1$, and $\Delta\tau = 0.01$.

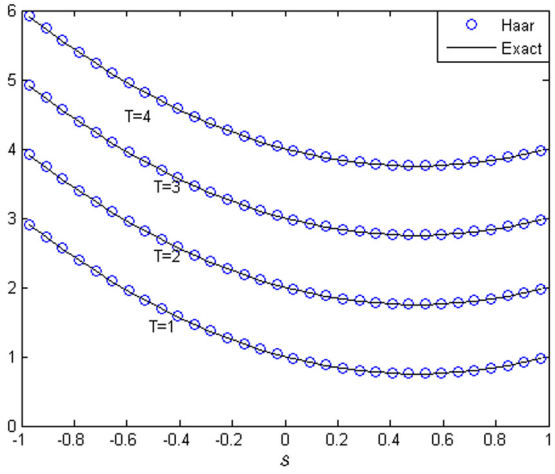

Figure 3: Comparison of exact and numerical solutions for Test Problem 3 at different T with $M = 16$ and $\Delta\tau = 0.01$.

solutions. The comparison of numerical and exact solutions at different T are also given in Figure 3. From these tables and figures it is concluded that the proposed HWCM can easily and accurately handle the first-order NLHPDE with various types of nonlinear terms.

Test Problem 4. We consider the following dissipative second-order NLHPDE [3,62]:

$$\frac{\partial^2\varphi}{\partial\tau^2} - \frac{\partial^2\varphi}{\partial s^2} + 2\varphi\frac{\partial\varphi}{\partial\tau} = (\pi^2 - 1 - 2\sin(\pi s)\sin(\tau))\sin(\pi s)\cos(\tau), \quad 0 \le s \le 1, \quad 0 \le \tau \le T,$$

with the initial conditions,

$$\varphi(s, 0) = \sin(\pi s) \quad \text{and} \quad \frac{\partial\varphi(s, 0)}{\partial\tau} = 0,$$

and the boundary conditions

$$\varphi(0, \tau) = 0 = \varphi(1, \tau).$$

The exact solution is

$$\varphi(s, \tau) = \sin(\pi s)\cos(\tau).$$

The 3D contours of exact and numerical solutions are compared in Figure 4, where the peaks appear by increasing the time T. The absolute errors are calculated for various time $T = 1, 7, 9, 12, 15$, and 19 and are presented graphically in Figure 5. In Table 9, we fixed $\Delta\tau = 0.0001$ for different values of M to check the spatial convergence of the HWCM, and it has been found that the theoretical and experimental rates of convergence for the space variable are in good agreement, and the CUP times are also shown. In Table 10, we fixed $M = 16$ and $T = 1$ for different $\Delta\tau$ to check the time variable convergence, where the theoretical and experimental rates of convergence for the time variable are also in good agreement. Hence, the HWCM is convergent and efficient.

Test Problem 5. We consider the following Klein-Gordon equation with two different cases as a challenging problem [63,64]:

$$\frac{\partial^2\varphi}{\partial\tau^2} - a_1^2\frac{\partial^2\varphi}{\partial s^2} + a_1\varphi - b_1\varphi^3 = 0, \quad -10 \le s \le 10, \quad 0 \le \tau \le T, \tag{23}$$

where $a_1, b_1 \in \mathbb{R}$, and $a_1 b_1 \neq 0$.

Case (i) (Single-soliton wave): Equation (23) represents a single-soliton wave if the initial conditions are

$$\varphi(s, 0) = A\text{sech}(Bs) \quad \text{and} \quad \frac{\partial\varphi(s, 0)}{\partial\tau} = c_o AB\text{sech}(Bs)\tanh(Bs),$$

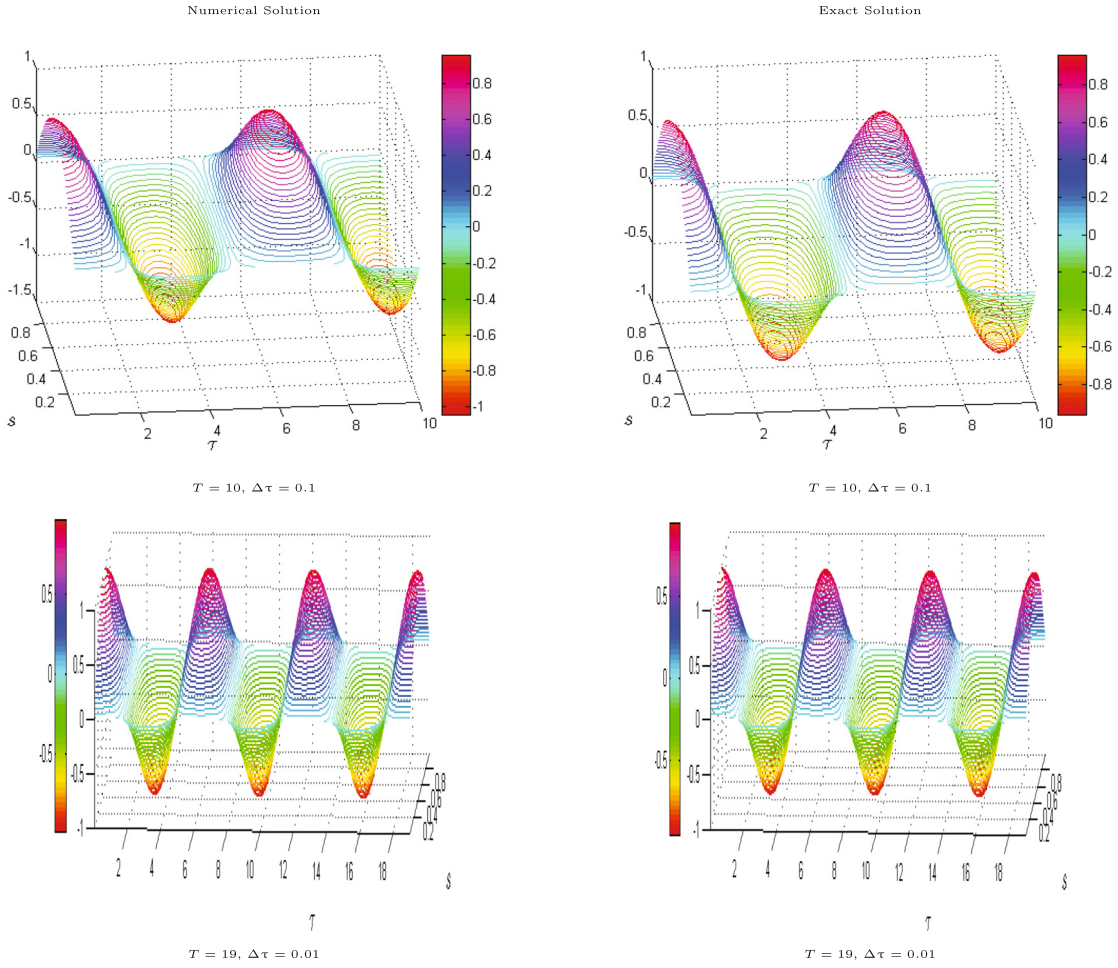

Figure 4: The 3D contour plots for Test Problem 4 at $M = 16$.

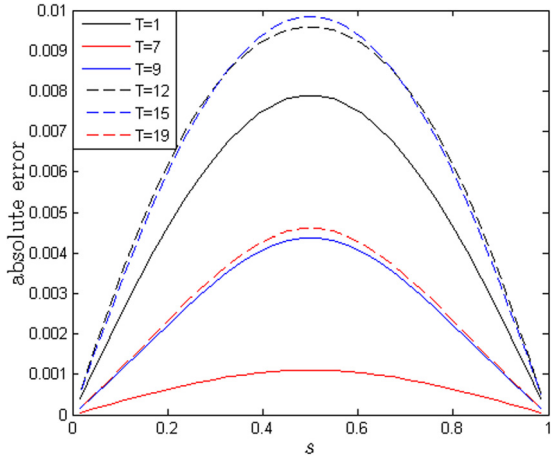

Figure 5: The absolute error for Test Problem 4 at different T with $M = 16$ and $\Delta\tau = 0.01$.

and the boundary conditions are

$$\varphi(0, \tau) = A\text{sech}(B(-10 - c_o\tau)) \quad \text{and} \quad \varphi(1, \tau) = A\text{sech}(B(10 - c_o\tau)).$$

Table 9: The numerical results at $\Delta\tau = 0.0001$, $a = 0$, $b = 1$, and $T = 1$ for Test Problem 4. The theoretical rate of convergence is 2 (Theorem 1)

M	E_∞	Experimental rate of convergence	CPU time (second unit)
1	7.5329×10^{-2}	—	2.7428
2	3.0358×10^{-2}	1.3111	5.6209
4	8.3629×10^{-3}	1.8600	11.1650
8	2.0812×10^{-3}	2.0065	24.4861
16	4.5977×10^{-4}	2.1784	41.5712

Table 10: The numerical results at $M = 16$, $a = 0$, $b = 1$, and $T = 1$ for Test Problem 4. The theoretical rate of convergence is 1 (Theorem 1)

$\Delta\tau$	E_∞	Experimental rate of convergence	CPU time (second unit)
1/10	7.5368×10^{-2}	—	1.3518
1/20	3.9613×10^{-2}	0.9279	1.4755
1/30	2.6765×10^{-2}	0.9669	1.8109
1/40	2.0146×10^{-2}	0.9874	2.3692
1/50	1.6110×10^{-2}	1.0019	2.7356
1/60	1.3391×10^{-2}	1.0137	3.1376
1/70	1.1435×10^{-2}	1.0241	3.6975
1/80	9.9613×10^{-2}	1.0336	4.1004
1/90	8.8100×10^{-2}	1.0427	4.5785
1/100	7.8861×10^{-2}	1.0514	5.0365

The exact solution is

$$\varphi(s, \tau) = A\text{sech}(B(s - c_o\tau)),$$

where $A = \sqrt{\frac{2a_1}{b_1}}$; $B = \frac{a_1}{a_1^2 - c_o^2}$; $a_1, b_1, a_1^2 - c_o^2 > 0$; c_o represents the velocity, and A is the wave amplitude. In our computation, we have considered $a_1 = 0.3$, $b_1 = 1$ and $c_o = 0.25$.

Case (ii) (Double-soliton wave): Equation (23) represents a double-soliton wave if the initial conditions are

$$\varphi(s, 0) = A\text{sech}[\mu_1(s - x_o)] + A\text{sech}[\mu_2(s - \acute{x}_o)] \quad \text{and}$$
$$\frac{\partial\varphi(s, 0)}{\partial\tau} = c_1\mu_1 A\text{sech}[\mu_1(s - x_o)]\tanh[\mu_1(s - x_o)] + c_2\mu_2 A\text{sech}[\mu_2(s - \acute{x}_o)]\tanh[\mu_2(s - \acute{x}_o)],$$

and the boundary conditions are

$$\varphi(-10, \tau) = A\text{sech}[\mu_1(-10 - x_o) - c_1\tau] + A\text{sech}[\mu_2(-10 - \acute{x}_o) - c_2\tau] \quad \text{and}$$
$$\varphi(10, \tau) = A\text{sech}[\mu_1(10 - x_o) - c_1\tau] + A\text{sech}[\mu_2(10 - \acute{x}_o) - c_2\tau].$$

The exact solution is

$$\varphi(s, \tau) = A\text{sech}[\mu_1(s - x_o) - c_1\tau] + A\text{sech}[\mu_2(s - \acute{x}_o) - c_2\tau],$$

where $A = \sqrt{\frac{2a_1}{b_1}}$ is the wave amplitude; $\mu_1 = \frac{a_1}{a_1^2 - c_1^2}$; $\mu_2 = \frac{a_1}{a_1^2 - c_2^2}$; and $a_1, b_1, a_1^2 - c_1^2, a_1^2 - c_2^2 > 0$. In our computation, we have considered $a_1 = 0.3$, $b_1 = 1$, $c_1 = -c_2 = 0.25$, $x_o = -2$, and $\acute{x}_o = 2$.

In Figure 6, the Haar wavelet based numerical solution is presented at different T and $\Delta\tau$ by fixing M, where the HWCM has easily captured the single soliton and there does not seem to be any blow-up phenomenon.

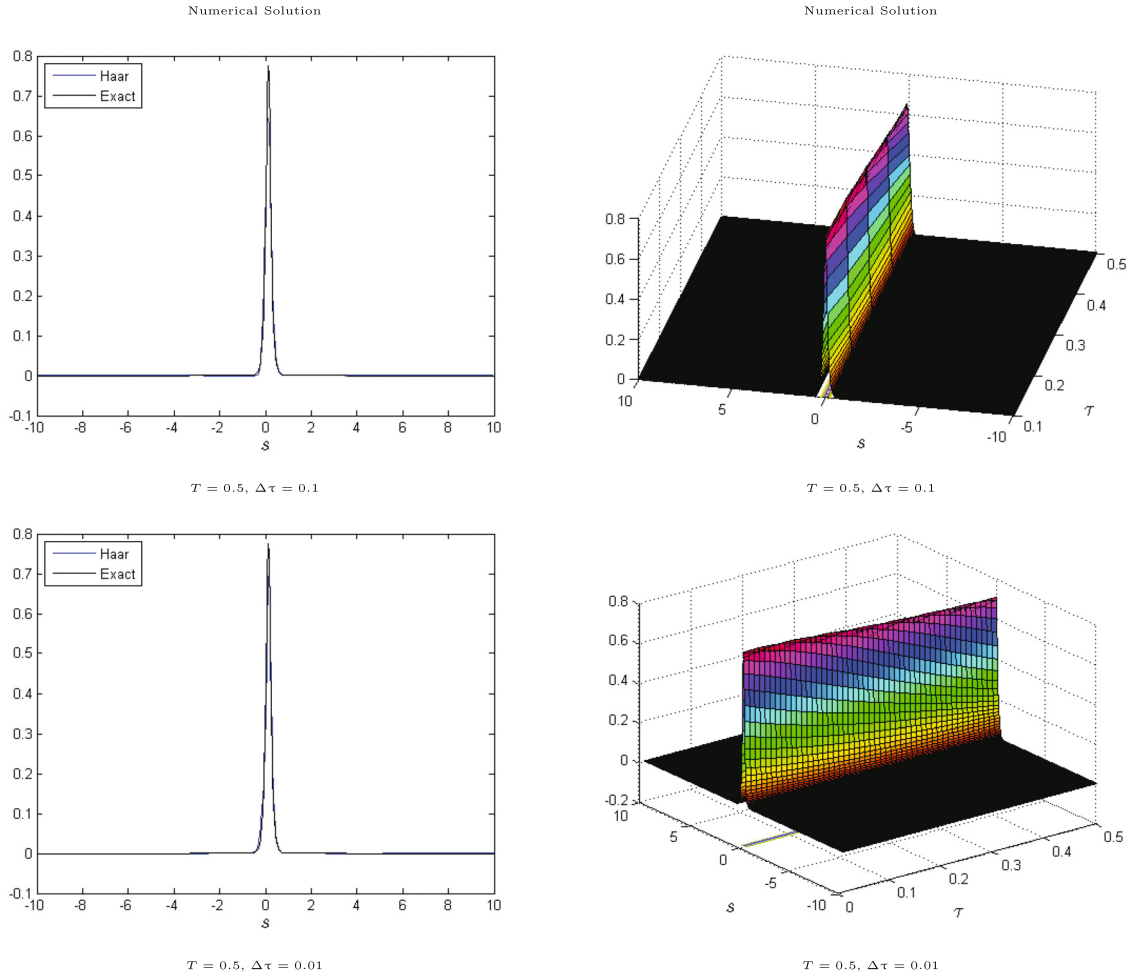

Figure 6: The numerical solution for Test Problem 5(i) at $M = 512$.

In Figure 7, the high resolution-based numerical solution is shown, where the HWCM captured the double soliton and also there does not seem to be any blow-up phenomenon, therefore the HWCM is stable. This example also illustrates the validity and capability of the proposed HWCM.

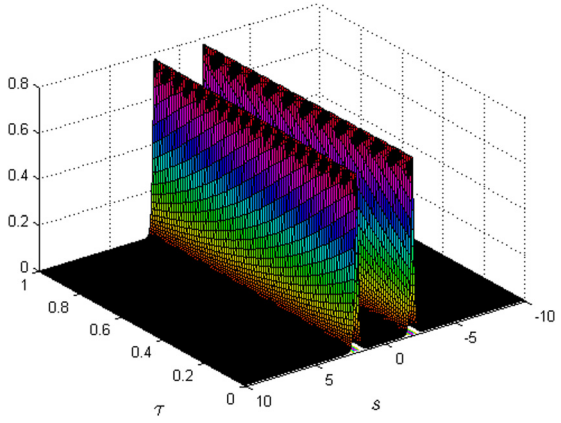

Figure 7: The numerical solutions for Test Problem 5(ii) at $T = 1$, $M = 512$, and $\Delta\tau = 0.01$.

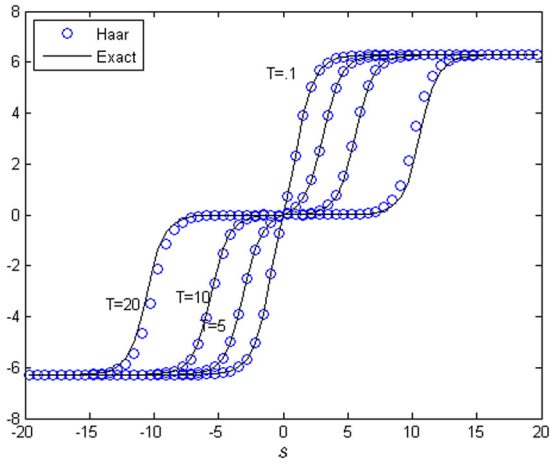

Figure 8: The comparison of exact and numerical solutions for Test Problem 6 at different T with $M = 16$ and $\Delta\tau = 0.01$.

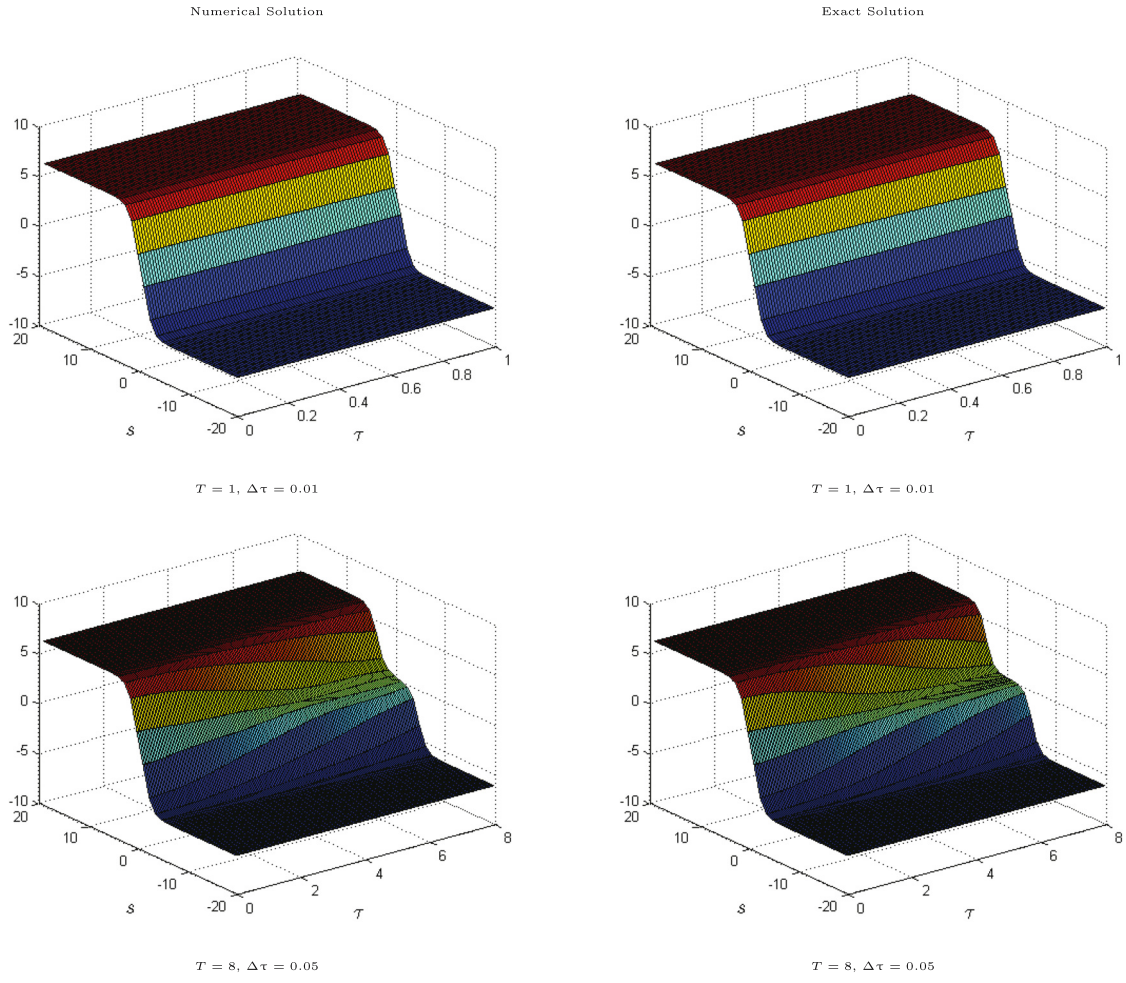

Figure 9: The 3D plots for Test Problem 6 at $M = 16$.

Test Problem 6. We consider the following Sine-Gordon equation as a special case of second-order NLHPDE

$$\frac{\partial^2\varphi}{\partial\tau^2} - \frac{\partial^2\varphi}{\partial s^2} + \sin(\varphi) = 0, \quad -20 \le s \le 20, \quad 0 \le \tau \le T.$$

The exact solution is given in [63]

$$\varphi(s,\tau) = 4\tan^{-1}\left(\frac{c_o \sinh\left(\frac{s}{\sqrt{1-c_o^2}}\right)}{\cosh\left(\frac{c_o\tau}{\sqrt{1-c_o^2}}\right)}\right).$$

The initial and boundary conditions can be obtained from the exact solution. For our numerical calculation, we have considered the velocity $c_o = 0.5$.

This Test Problem is challenging and represents the collision of two Sine-Gordon kink solitons. In Figure 8, the comparison of the exact and numerical solutions for different time $T = 0.1$, 5, 10, and 20 are shown and the collision of kink solitons can be clearly observed. The 3D view of the numerical and exact solution up to $T = 8$ is presented in Figure 9. In Table 11, we fixed $\Delta\tau = 0.0001$ for different values of M to check the spatial convergence of the HWCM, and it has been found that the theoretical and experimental rates of convergence for the space variable are in good agreement. The numerical results at $M = 16$ and $T = 1$ for different $\Delta\tau$ are given in Table 12, where the theoretical and experimental rates of convergence for the time variable are also in good agreement in this case.

Table 11: The numerical results at $\Delta\tau = 0.0001$, $a = 0$, $b = 1$, and $T = 1$ for Test Problem 6. The theoretical rate of convergence is 2 (Theorem 1)

M	E_∞	Experimental rate of convergence	CPU time (second unit)
1	4.5990×10^{-3}	—	2.4199
2	2.3806×10^{-3}	0.9499	5.4584
4	6.9063×10^{-4}	1.7853	15.5490
8	2.0234×10^{-4}	1.7710	55.3128

Table 12: The numerical results at $M = 16$, $a = 0$, $b = 1$, and $T = 1$ for Test Problem 6. The theoretical rate of convergence is 1 (Theorem 1)

$\Delta\tau$	E_∞	Experimental rate of convergence
1/10	0.0562	—
1/20	0.0261	0.9721
1/30	0.0175	0.9847
1/40	0.0132	0.9893
1/50	0.0105	0.9917
1/60	0.0088	0.9932
1/70	0.0075	0.9942
1/80	0.0066	0.9949
1/90	0.0059	0.9954
1/100	0.0053	0.9958

6 Conclusion

In this work, we have proposed the HWCM for the numerical solution of the first- and second-order NLHPDEs. The E_∞ error norm and the rate of convergence show that the proposed numerical method is accurate and applicable to solve NLHPDEs. Considering the different types of nonlinear equations discussed earlier, we may conclude that the proposed HWCM is practical, efficient, and effective for solving the first- and second-order NlHPDEs numerically. Due to the high potential achievements of the HWCM, the current scheme can be implemented to 2D and coupled NLHPDEs. These topics are the focus of our forthcoming work.

Funding information: The first author would like to acknowledge the financial support from the research grants: 2020B1515120083 by the Guangdong Basic and Applied Basic Research Foundation and JCYJ20210324121402008 by the Shenzhen Science and Technology Innovation Commission. The corresponding author (Zaheer Uddin) is thankful to the CECOS University for research encouragement.

Author contributions: All authors have equally contributed to finalizing the article.

Conflict of interest: The authors declare that there is no conflict of interest.

Data availability statement: Not applicable.

References

[1] E. H. Doha, R. M. Hafez, and Y. H. Youssri, *Shifted Jacobi spectral-Galerkin method for solving hyperbolic partial differential equations*, Comput. Math. Appl. **78** (2019), no. 3, 889–904.

[2] S. Singh, V. Kumar Patel, and V. K. Singh, *Application of wavelet collocation method for hyperbolic partial differential equations via matrices*, Appl. Math. Comput. **320** (2018), 407–424.

[3] S. N. Jator, F. F. Ngwane, and N. O. Kirby, *Functionally fitted block method for solving the general oscillatory second-order initial value problems and hyperbolic partial differential equations*, Math. Prob. Eng. **2019** (2019), 1–14.

[4] J. Banasiak and J. R. Mika, *Singularly perturbed telegraph equations with applications in the random walk theory*, J. Appl. Math. Stoch. Anal. **11** (1998), no. 1, 9–28.

[5] V. H. Weston and S. He, *Wave splitting of the telegraph equation in R3 and its application to inverse scattering*, Inv. Prob. **9** (1993), no. 6, 789.

[6] L.-B. Liu and H.-W. Liu, *Compact difference schemes for solving telegraphic equations with Neumann boundary conditions*, Appl. Math. Comput. **219** (2013), no. 19, 10112–10121.

[7] H. Moghaderi and M. Dehghan, *A multigrid compact finite difference method for solving the one-dimensional nonlinear Sine-Gordon equation*, Math. Methods Appl. Sci. **38** (2015), no. 17, 3901–3922.

[8] J. Rashidinia and R. Mohammadi, *Tension spline solution of nonlinear Sine-Gordon equation*, Numer. Alg. **56** (2011), no. 1, 129–142.

[9] W. Bao, Y. Feng, and W. Yi, *Long time error analysis of finite difference time domain methods for the nonlinear Klein-Gordon equation with weak nonlinearity*, Commun. Comput. Phys **26** (2019), 1307–1334.

[10] Y. Luo, X. Li, and C. Guo, *Fourth-order compact and energy conservative scheme for solving nonlinear Klein-Gordon equation*, Numer. Methods Partial Differential Equations **33** (2017), no. 4, 1283–1304.

[11] A. G. Atta, W. M. Abd-Elhameed, G. M. Moatimid, and Y. H. Youssri, *Shifted fifth-kind Chebyshev Galerkin treatment for linear hyperbolic first-order partial differential equations*, Appl. Numer. Math. **167** (2021), 237–256.

[12] W. M. Abd-Elhameed, E. H. Doha, Y. H. Youssri, and M. Bassuony, *New Tchebyshev-Galerkin operational matrix method for solving linear and nonlinear hyperbolic telegraph type equations*, Numer. Methods Partial Differential Equations **32** (2016), no. 6, 1553–1571.

[13] Ş. Yüzbaşı and M. Karaçayır, *A Galerkin-type method to solve one-dimensional telegraph equation using collocation points in initial and boundary conditions*, Int. J. Comput. Methods **15** (2018), no. 5, 1850031.

[14] R. C. Mittal and R. Bhatia, *Numerical solution of nonlinear Sine-Gordon equation by modified cubic B-spline collocation method*, Int. J. Partial Differential Equations **2014** (2014), 1–8.

[15] W. Liu, B. Wu, and J. Sun, *Space-time spectral collocation method for the one-dimensional Sine-Gordon equation*, Numer. Methods Partial Differential Equations **31** (2015), no. 3, 670–690.
[16] Y. H. Youssri and R. M. Hafez, *Exponential Jacobi spectral method for hyperbolic partial differential equations*, Math. Sci. **13** (2019), no. 4, 347–354.
[17] A. G. Atta, W. M. Abd-Elhameed, G. M. Moatimid, and Y. H. Youssri, *Advanced shifted sixth-kind Chebyshev tau approach for solving linear one-dimensional hyperbolic telegraph type problem*, Math. Sci. (2022), 1–15, DOI: https://doi.org/10.1007/s40096-022-00460-6.
[18] Q. Jin and W. Wang, *Analysis of the iteratively regularized Gauss-Newton method under a heuristic rule*, Inverse Problems **34** (2018), no. 3, 1–24.
[19] Q. Jin, *On a heuristic stopping rule for the regularization of inverse problems by the augmented Lagrangian method*, Numer. Math. **136** (2017), no. 4, 973–992.
[20] Q. Jin and X. Lu, *A fast nonstationary iterative method with convex penalty for inverse problems in Hilbert spaces*, Inverse Problems **30** (2014), no. 4, 1–21.
[21] Y. Liu, Y. Liu, and Z. Cen, *Daubechies wavelet meshless method for 2-D elastic problems*, Tsinghua Sci. Tech. **13** (2008), no. 5, 605–608.
[22] L. A. Diiiaz, M. T. Martiiin, and V. Vampa, *Daubechies wavelet beam and plate finite elements*, Finite Elem. Anal. Des. **45** (2009), no. 3, 200–209.
[23] G.-W. Jang, Y. Y. Kim, and K. K. Choi, *Remesh-free shape optimization using the wavelet-Galerkin method*, Int. J. Sold. Struc. **41** (2004), no. 22, 6465–6483.
[24] Siraj-ul-Islam, I. Aziz, and A. S. Al-Fhaid, *An improved method based on Haar wavelets for numerical solution of nonlinear integral and integro-differential equations of first and higher orders*, J. Comput. Appl. Math. **260** (2014), 449–469.
[25] M. Ahsan, M. Bohner, A. Ullah, A. A. Khan, and S. Ahmad, *A Haar wavelet multi-resolution collocation method for singularly perturbed differential equations with integral boundary conditions*, Math. Comput. Simulation **204** (2023), 166–180.
[26] W. Dahmen, A. J. Kurdila, and P. Oswald (eds.), Multiscale wavelet methods for partial differential equations, *Wavelet Analysis and its Applications*, vol. 6, Academic Press, Inc., San Diego, CA, 1997.
[27] T. Tran, E. P. Stephan, and P. Mund, *Hierarchical basis preconditioners for first kind integral equations*, Appl. Anal. **65** (1997), no. 3–4, 353–372.
[28] K. Maleknejad and F. Mirzaee, *Using rationalized Haar wavelet for solving linear integral equations*, Appl. Math. Comput. **160** (2005), no. 2, 579–587.
[29] U. Lepik, *Haar wavelet method for nonlinear integro-differential equations*, Appl. Math. Comput. **176** (2006), no. 1, 324–333.
[30] Siraj-ul-Islam, M. Ahsan, and I. Hussian, *A multi-resolution collocation procedure for time-dependent inverse heat problems*, Int. J. Therm. Sci. **128** (2018), 160–174.
[31] M. Ahsan, I. Ahmad, M. Ahmad, and I. Hussian, *A numerical Haar wavelet-finite difference hybrid method for linear and non-linear Schrödinger equation*, Math. Comput. Simulation **165** (2019), 13–25.
[32] C.-H. Hsiao and W.-J. Wang, *Haar wavelet approach to nonlinear stiff systems*, Math. Comput. Simulation **57** (2001), no. 6, 347–353.
[33] F. A. Shah, R. Abass, and J. Iqbal, *Numerical solution of singularly perturbed problems using Haar wavelet collocation method*, Cogent Math. **3** (2016), Art. 1202504, 13.
[34] F. A. Shah and R. Abass, *An operational Haar wavelet collocation method for solving singularly perturbed boundary-value problems*, SeMA J. Bol. Soci. Espan. Matem. Apli. **74** (2017), no. 4, 457–474.
[35] G. Rana, M. Asif, N. Haider, R. Bilal, M. Ahsan, Q. Al-Mdallal, et al., *A modified algorithm based on Haar wavelets for the numerical simulation of interface models*, J. Funct. Spaces **2022** (2022), 1–15.
[36] I. Aziz, Siraj-ul-Islam, and F. Khan, *A new method based on Haar wavelet for the numerical solution of two-dimensional nonlinear integral equations*, J. Comput. Appl. Math. **272** (2014), 70–80.
[37] Siraj-ul-Islam, I. Aziz, and F. Haq, *A comparative study of numerical integration based on Haar wavelets and hybrid functions*, Comput. Math. Appli. **59** (2010), no. 6, 2026–2036.
[38] I. Aziz, Siraj-ul-Islam, and B. Šarler, *Wavelets collocation methods for the numerical solution of elliptic BV problems*, Appl. Math. Model. **37** (2013), no. 3, 676–694.
[39] M. Ahsan, W. Lei, M. Ahmad, M. S. Hussein, and Z. Uddin, *A wavelet-based collocation technique to find the discontinuous heat source in inverse heat conduction problems*, Phys. Scr. **97** (2022), no. 12, 125208.
[40] Siraj-ul-Islam, I. Aziz, and M. Ahmad, *Numerical solution of two-dimensional elliptic PDEs with nonlocal boundary conditions*, Comput. Math. Appl. **69** (2015), no. 3, 180–205.
[41] M. Ahsan, Siraj-ul-Islam, and I. Hussain, *Haar wavelets multi-resolution collocation analysis of unsteady inverse heat problems*, Inverse Probl. Sci. Engrg. **27** (2019), no. 11, 1498–1520.
[42] M. Ahsan, M. Ahmad, W. Khan, E. E. Mahmoud, and A.-H. Abdel-Aty, *Meshless analysis of nonlocal boundary value problems in anisotropic and inhomogeneous media*, Mathematics **8** (2020), no. 11, 2045.

[43] J. Majak, B. Shvartsman, M. Pohlak, K. Karjust, M. Eerme, and E. Tungel, *Solution of fractional order differential equation by the Haar wavelet method. Numerical convergence analysis for most commonly used approach*, AIP Conference Proceedings, vol. 1738, AIP Publishing LLC, 2016, p. 480110.
[44] Y. Li and W. Zhao, *Haar wavelet operational matrix of fractional order integration and its applications in solving the fractional order differential equations*, Appl. Math. Comput. **216** (2010), no. 8, 2276–2285.
[45] M. Yi and J. Huang, *Wavelet operational matrix method for solving fractional differential equations with variable coefficients*, Appl. Math. Comput. **230** (2014), 383–394.
[46] U. Saeed and M. ur Rehman, *Haar wavelet Picard method for fractional nonlinear partial differential equations*, Appl. Math. Comput. **264** (2015), 310–322.
[47] L. Wang, Y. Ma, and Z. Meng, *Haar wavelet method for solving fractional partial differential equations numerically*, Appl. Math. Comput. **227** (2014), 66–76.
[48] X. Liu, M. Ahsan, M. Ahmad, I. Hussain, M. M. Alqarni, and E. E. Mahoud, *Haar wavelets multi-resolution collocation procedures for two-dimensional nonlinear Schrödinger equation*, Alex. Eng. J. **60** (2021), no. 3, 3057–3071.
[49] X. Liu, M. Ahsan, M. Ahmad, M. Nisar, X. Liu, I. Ahmad, et al., *Applications of Haar wavelet-finite difference hybrid method and its convergence for hyperbolic nonlinear Schrödinger equation with energy and mass conversion*, Energies **14** (2021), no. 23, 1–17, Art. ID 7831.
[50] M. Ahsan, T. Tran, Siraj-ul-Islam, and I. Hussain, *A multiresolution collocation method and its convergence for Burgers' type equations*, Math. Methods Appl. Sci. (2022), 1–24, DOI: https://doi.org/10.1002/mma.8764.
[51] M. Ahsan, S. Lin, M. Ahmad, M. Nisar, I. Ahmad, H. Ahmed, et al., *A Haar wavelet-based scheme for finding the control parameter in nonlinear inverse heat conduction equation*, Open Phys. **19** (2021), no. 1, 722–734.
[52] M. Ahsan, I. Hussain, and M. Ahmad, *A finite-difference and Haar wavelets hybrid collocation technique for non-linear inverse Cauchy problems*, Appl. Math. Sci. Eng. **30** (2022), no. 1, 121–140.
[53] M. Ahsan, K. Shams-ul-Haq, X. Liu, S. Ahmad, and M. Nisar, *A Haar wavelets based approximation for nonlinear inverse problems influenced by unknown heat source*, Math. Methods Appl. Sci. **46** (2023), no. 2, 2475–2487.
[54] S. Nazir, S. Shahzad, R. Wirza, R. Amin, M. Ahsan, N. Mukhtar, et al., *Birthmark based identification of software piracy using Haar wavelet*, Math. Comput. Simulation **166** (2019), 144–154.
[55] S. M. Aznam and M. S. Chowdhury, *Generalized Haar wavelet operational matrix method for solving hyperbolic heat conduction in thin surface layers*, Results Phys. **11** (2018), 243–252.
[56] S. Pandit, R. Jiwari, K. Bedi, and M. E. Koksal, *Haar wavelets operational matrix based algorithm for computational modelling of hyperbolic type wave equations*, Eng. Comput. **34** (2017), no. 8, 2793–2814.
[57] R. K. Mohanty, *New unconditionally stable difference schemes for the solution of multi-dimensional telegraphic equations*, Int. J. Comput. Math. **86** (2009), no. 12, 2061–2071.
[58] W. Greiner, *Relativistic Quantum Mechanics*, vol. 2, Springer, Berlin, 2000.
[59] A. Scott, *Nonlinear Science: Emergence and Dynamics of Coherent Structures*, Oxford University Press, Oxford, 2003.
[60] T. Dauxois and M. Peyrard, *Physics of Solitons*, Cambridge University Press, Cambridge, 2006.
[61] J. Majak, B. S. Shvartsman, M. Kirs, M. Pohlak, and H. Herranen, *Convergence theorem for the Haar wavelet based discretization method*, Compos. Struct. **126** (2015), 227–232.
[62] R. Jiwari, *Lagrange interpolation and modified cubic B-spline differential quadrature methods for solving hyperbolic partial differential equations with Dirichlet and Neumann boundary conditions*, Comput. Phys. Commun. **193** (2015), 55–65.
[63] A. Mohebbi and M. Dehghan, *High-order solution of one-dimensional Sine-Gordon equation using compact finite difference and DIRKN methods*, Math. Comput. Modell. **51** (2010), no. 5–6, 537–549.
[64] Y. Duan, L. Kong, and M. Guo, *Numerical simulation of a class of nonlinear wave equations by lattice Boltzmann method*, Commun. Math. Stat. **5** (2017), no. 1, 13–35.